

Coupling induced anomalous group velocity dispersion in nonlinear arrays of silicon photonic wires

Christopher J. Benton and Dmitry V. Skryabin

*Centre for Photonics and Photonic Materials,
Department of Physics, University of Bath, Bath, BA2 7AY, United Kingdom*
d.v.skryabin@bath.ac.uk

Abstract: We demonstrate that the group velocity dispersion (GVD) of the supermodes in a small array of silicon photonic wires can differ dramatically from the single wire GVD. This enables soliton propagation and modulational instability to be seen at wavelengths where single wires have strongly normal GVD.

© 2009 Optical Society of America

OCIS codes: 050.1940, 080.1238, 130.5990, 190.5530, 260.2030.

References and links

1. M. A. Foster, A. C. Turner, M. Lipson, and A. L. Gaeta. Nonlinear optics in photonic nanowires. *Opt. Express* **16**, 1300–1320 (2008).
2. Q. Lin, O. J. Painter, and G. P. Agrawal. Nonlinear optical phenomena in silicon waveguides: modeling and applications. *Opt. Express* **15**, 16604–16644 (2007).
3. M. Hochberg, T. Baehr-Jones, G. Wang, and M. Shearn. Terahertz all-optical modulation in a silicon-polymer hybrid system. *Nature Mater.* **5**, 703–709 (2006).
4. M. A. Foster, A. C. Turner, J. E. Sharping, B. S. Schmidt, M. Lipson, and A. L. Gaeta. Broad-band optical parametric gain on a silicon photonic chip. *Nature* **441**, 960–963 (2006).
5. V. R. Almeida, C. A. Barrios, R. R. Panepucci, and M. Lipson. All-optical control of light on a silicon chip. *Nature* **431**, 1081–1084 (2004).
6. Y. Vlasov, W. M. J. Green, and F. Xia. High-throughput silicon nanophotonic wavelength-insensitive switch for on-chip optical networks. *Nat. Photonics* **2**, 242–246 (2008).
7. Q. Lin, J. Zhang, G. Piredda, R. W. Boyd, P. M. Fauchet, and G. P. Agrawal. Dispersion of silicon nonlinearities in the near infrared region. *Appl. Phys. Lett.* **91**, 021111 (2007).
8. A. C. Turner, C. Manolatou, B. S. Schmidt, M. Lipson, M. A. Foster, J. E. Sharping, and A. L. Gaeta. Tailored anomalous group-velocity dispersion in silicon channel waveguides. *Opt. Express* **14**, 4357–4362 (2006).
9. E. Dulkeith, F. Xia, L. Schares, W.M. J. Green, and Y. A. Vlasov. Group index and group velocity dispersion in silicon-on-insulator photonic wires. *Opt. Express* **14**, 3853–3863 (2006).
10. E. Dulkeith, Y. A. Vlasov, X. Chen, N. C. Panoiu, and R. M. Osgood. Self-phase-modulation in submicron silicon-on-insulator photonic wires. *Opt. Express* **14**, 5524–5534 (2006).
11. W. Ding, C. Benton, A. V. Gorbach, W. J. Wadsworth, J. C. Knight, D. V. Skryabin, M. Gnan, M. Sorrel, and R. M. De-La-Rue. Solitons and spectral broadening in long silicon-on-insulator photonic wires. *Opt. Express* **16**, 3310–3319 (2008).
12. J. Zhang, Q. Lin, G. Piredda, R. W. Boyd, G. P. Agrawal, and P. M. Fauchet. Optical solitons in a silicon waveguide. *Opt. Express* **15**, 7682–7688 (2007).
13. J. I. Dadap, N. C. Panoiu, X. Chen, I.W. Hsieh, X. Liu, C.Y. Chou, E. Dulkeith, S. J. McNab, F. Xia, W. M. J. Green, L. Sekaric, Y. A. Vlasov, and Jr. R. M. Osgood. Nonlinear-optical phase modification in dispersion-engineered silicon photonic wires. *Opt. Express* **16**, 1280–1299 (2008).
14. T. Pertsch, T. Zentgraf, U. Peschel, A. Bruer, and F. Lederer. Anomalous refraction and diffraction in discrete optical systems. *Phys. Rev. Lett.* **88**, 093901 (2002).
15. F. Lederer, G.I. Stegeman, D.N. Christodoulides, G. Assanto, M. Segev, and Y. Silberberg. Discrete solitons in optics. *Phys. Rep.* **463**, 1-126 (2008).

16. A. V. Yulin, D. V. Skryabin, and A. G. Vladimirov. Modulational instability of discrete solitons in coupled waveguides with group velocity dispersion. *Opt. Express* **14**, 12347–12352 (2006).
17. P. D. Rasmussen, A. A. Sukhorukov, D. N. Neshev, W. Krolikowski, O. Bang, J. Lagsgaard, and Y. S. Kivshar. Spatiotemporal control of light by bloch-mode dispersion in multi-core fibers. *Opt. Express* **16**, 5878–5891 (2008).
18. C. J. Benton, A. V. Gorbach, and D. V. Skryabin. Spatiotemporal quasisolitons and resonant radiation in arrays of silicon-on-insulator photonic wires. *Phys. Rev. A* **78**, 033818 (2008).
19. K. S. Chiang, Y. T. Chow, D. J. Richardson, D. Taverner, L. Dong, L. Reekie, and K. M. Lo. Experimental demonstration of intermodal dispersion in a two-core optical fibre. *Opt. Commun.* **143**, 189–192 (1997).
20. M. Yu, C. J. McKinstrie, and G. P. Agrawal. Modulational instabilities in dispersion-flattened fibers. *Phys. Rev. E* **52**, 1072–1080 (1995).
21. F. Biancalana, D. V. Skryabin, and P. S. Russell. Four-wave mixing instabilities in photonic-crystal and tapered fibers. *Phys. Rev. E* **68**, 046603 (2003).
22. N. Akhmediev and A. Ankiewicz. Novel soliton states and bifurcation phenomena in nonlinear fiber couplers. *Phys. Rev. Lett.* **70**, 2395–2398 (1993).

Dispersion control is one of central issues in the design of nonlinear optical waveguides. Important phenomena such as supercontinuum generation and parametric frequency conversion in optical fibers depend greatly on the engineering of the dispersion relation. High index optical materials can confine light to scales similar to or less than the wavelength, which can alter both the magnitude and the sign of the group-velocity dispersion. Silicon has recently received a great deal of attention as the material of choice for building practical optical information processing devices [1, 2]. In particular, nano-sized silicon-on-insulator (SOI) photonic wires have been considered as building blocks in nonlinear modulation devices [3], on-chip frequency converters [4], and other applications [5, 6]. The large Kerr nonlinearity of silicon [7] combined with the strong anomalous dispersion that can be achieved in photonic wires [8, 9] has enabled the observation at low power of self-phase modulation [10, 11], modulational instability [4] and quasi-solitons [11, 12] over microchip lengthscales.

The engineering of GVD in isolated silicon photonic wires by changing their height, width and cladding has received recent attention [8, 13]. Here we study a different approach to GVD control. We consider the evanescent field coupling between several silicon wires in the regime where the wire width and spacing width are both much less than the free space wavelength ($1.5\mu\text{m}$). In this regime, the coupling between the wires becomes strongly dispersive, but remains evanescent. The array of N wires naturally supports N different modes (or supermodes). As a result of the coupling dispersion, the GVD of the supermodes deviate significantly from the single wire GVD. This, for example, leads to the situation where the GVD in a single wire is large and normal, whilst a directional coupler of 2 wires (or an array of $N > 2$ wires) support supermodes with large ($\sim 10^3\text{ps/nm/km}$) anomalous GVD. These values allow for the observation of femtosecond solitons and modulational instability, which would not be expected for a single wire. The selection of a particular supermode in the array structures can be achieved by an excitation at an appropriate angle, which is a well known method used for control of the 'discrete' diffraction [14, 15]. The interplay of diffraction and dispersion in nonlinear waveguide arrays has been studied previously, see e.g. [15, 16, 17, 18] and references therein, but the distinct feature of our study is the important role played by the dispersion of the discrete diffraction coefficient.

The structures we are considering here are 220nm high and 330nm wide rectangular wires sitting atop a silica slab, with a 100nm etching mask (of refractive index 1.35) above, and otherwise surrounded by air. The wire-to-wire separation of 330nm gives strongly dispersive coupling in the proximity of $\lambda_0 = 1.5\mu\text{m}$. The corresponding field profiles of the in-phase and anti-phase TE modes of a directional coupler consisting of two such wires were calculated by solving Maxwell equations, as is shown in Fig. 1(a). Despite the relatively small separation, the two modes still can be well approximated as the in-phase and anti-phase superpositions of the modes

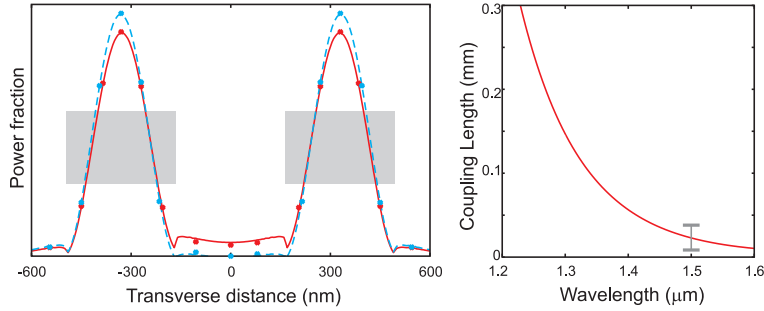


Fig. 1. (a) Supermodes of the directional coupler, shown as transmitted power as function of transverse distance. The red (blue) line shows the symmetric (antisymmetric) supermode. The wire dimensions are shown overlaid. The dots show linear superpositions of the single-wire modes, confirming the validity of our use of this approximation. (b) Coupling length L_c as a function of λ for the structures shown in (a).

of a single wire, see Fig. 1(a). The dispersions of the two modes are given by the frequency dependencies of their propagation constants β_s and β_a , respectively. These dependencies were calculated numerically and fitted with 11th order polynomials $\beta_\times(\omega) = \sum_{m=0}^{11} \frac{1}{m!} \beta_{\times m} \omega^m$ (where β_\times may represent β_s or β_a), and $\omega = \Omega - \Omega_0$ is the detuning of the frequency Ω from the pump at $\Omega_0 = 2\pi c/\lambda_0$. The propagation constant of a single uncoupled wire is very well approximated by $\beta(\omega) = \sum_{m=0}^{11} \frac{1}{m!} \beta_m \omega^m$, where $\beta_m = \frac{1}{2}(\beta_{sm} + \beta_{am})$. The coupling coefficient between the wires is defined as $K(\omega) = \sum_{m=0}^{11} \frac{1}{m!} \kappa_m \omega^m$, where $\kappa_m = \frac{1}{2}(\beta_{sm} - \beta_{am})$ [18]. Figure 1(b) shows the wavelength (λ) dependence of the coupling length $L_c = \pi/K$. One can see that for the chosen geometry the coupling is very strong and energy is transferred from one waveguide to another after only a few tens of microns.

A particularly important parameter for our purposes is the dispersion parameter of the coupling, which is defined as $-(\omega^2/2\pi c) \partial_\omega^2 K$. Comparing the coupling induced dispersion (the full line in Fig. 2(a)) with the dispersion in a single wire ($-(\omega^2/2\pi c) \partial_\omega^2 \beta$, the full line in Fig. 2(b)), one can see that the former can be comparable in absolute value to the latter over

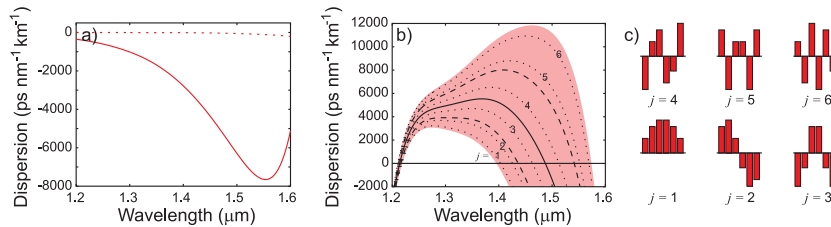


Fig. 2. (a) The full line shows the coupling dispersion $-(\omega^2/2\pi c) \partial_\omega^2 K$ for $220\text{nm} \times 330\text{nm}$ wires with a 330nm gap. The dashed line shows the same, but for $220\text{nm} \times 420\text{nm}$ wires with a 700nm gap. (b) The full line is the dispersion $-(\omega^2/2\pi c) \partial_\omega^2 D$ of an isolated $220 \times 330\text{nm}$ wire. The dashed lines are the dispersions of the in-phase (below the full line) and anti-phase (above the full line) modes of the coupler. The dotted lines are the dispersions of supermodes in the 6-wire array. The shaded area spans the region between the dispersions of the in-phase and out-of-phase modes of an infinite array. The wire size for (b) is $230 \times 330\text{nm}$. (c) The linear supermodes for a six wire array. The index j in (b) and (c) corresponds to that in Eq. 2

the wavelength range of interest. By way of comparison, the dashed line in Fig. 2(a) shows the coupling dispersion for 220nm \times 420nm wires separated by 700nm, as were studied in [18], revealing a significant drop in the values of the coupling dispersion for a relatively small change in geometry.

We modelled the arrays of silicon photonic wires using a set of dimensionless coupled non-linear Schrödinger equations

$$\partial_z E_n - i\hat{D}(i\partial_t)E_n = i\hat{C}(i\partial_t)(E_{n-1} + E_{n+1}) + i(1 + i\varepsilon_{\text{tpa}})|E_n|^2 E_n - (\varepsilon + \varepsilon_{fc}Q_n)E_n, \quad (1)$$

where $n = 1, 2, \dots, N$. Here E_n is the amplitude of the electric field in the n th wire of an N -wire array. Time is given by t (in units of $T_0 = 56.7$ fs, such that $\text{sech}^2(t)$ gives a 100fs FWHM pulse), whilst distance along the wires is given by z (in units of the dispersion length (at 100fs) $L_D \equiv T_0^2/|\beta_2| = 1.93$ mm). The dispersion operator for a single wire is defined as $\hat{D}(i\partial_t) = \sum_{m=2}^{11} d_m (i\partial_t)^m$ where $d_m \equiv \beta_m L_D / m! T_0^m$. Coupling and its dispersion are represented by the operator $\hat{C}(i\partial_t) = \sum_{m=0}^{11} c_m (i\partial_t)^m$ where $c_m \equiv \kappa_m L_D / m! T_0^m$. The absorption length is given by $1/\varepsilon \simeq 40$ mm. Power is scaled such that $P_0 |E_n|^2$ gives the physical power in the n th wire, where $P_0 = (L_D \gamma)^{-1}$. Assuming $\gamma \simeq 500 \text{ m}^{-1} \text{ W}^{-1}$, gives $P_0 \simeq 1$ W. The ratio of the TPA coefficient to the Kerr nonlinearity was assumed to be $\varepsilon_{\text{tpa}} = 0.1$ [11]. The free carrier density in the n th waveguide is given by Q_n , which is measured in units of $T_0 \varepsilon_{\text{tpa}} / L_D^2 \gamma \hbar \omega S_{\text{eff}}$, and obeys $\partial_t Q_n = |E|^4 - Q_n / \tau_c$. The carrier lifetime τ_c (which is typically of the order 10ns) was assumed to be much longer than the pulse length (which for our purposes never exceeds 10ps), but much shorter than the repetition length (such that decay is negligible between pulses, but total between them). The carrier cross section is represented as $\varepsilon_{fc} = \varepsilon_{\text{tpa}} T_0 \sigma_{fc} / 2 \hbar \omega S_{\text{eff}} \gamma L_D$, where $\sigma_{fc} = 1.45 \times 10^{-21} (1 + 7.5i) \text{ m}^2$ is the complex absorption and scattering cross section in physical units, S_{eff} is the effective waveguide area, and $\hbar \omega$ is the photon energy. This quantity is vulnerable to the uncertainties in S_{eff} and γ . Assuming that S_{eff} is half the physical area of the waveguide, gives an estimate of $\varepsilon_{fc} \simeq 10^{-3} (1 + 7.5i)$.

For femtosecond pulses, the effects of free carriers on a single pulse excitation are negligible and Q_n can be safely assumed zero. However, for the 10ps pulses we use to observe modulational instability, a full account for the free carrier dynamics is essential.

In order to gain an analytical insight into modulational instability and soliton propagation, we neglect linear loss, TPA and free carrier terms. Working in the supermode basis formally eliminates the linear coupling terms from the equations, making the calculations more transparent. Introducing the vector $\vec{E} = (E_1, \dots, E_N)^T$, we find that the linear part of Eqs. (1) is represented as $[\partial_z - i\hat{D}] \vec{E} = i\hat{X}\hat{C}\vec{E}$, where \hat{X} is the $N \times N$ matrix with elements $X_{n,j} = \delta_{n,j-1} + \delta_{n,j+1}$, where δ is the Kronecker symbol and $j = 1, \dots, N$. We expand \vec{E} into this supermode basis as $\vec{E} = \sqrt{2(N+1)/3} \sum_{j=1}^N \tilde{E}_j \vec{x}_j$, where \vec{x}_j are the normalized eigenvectors of \hat{X} , which are the supermodes. The supermode amplitudes \tilde{E}_j obey

$$\partial_z \tilde{E}_j - i\hat{D}_j(i\partial_t)\tilde{E}_j = i\Gamma_{Nj} |\tilde{E}_j|^2 \tilde{E}_j + f_{Nj}(\tilde{E}_1, \tilde{E}_2, \dots, \tilde{E}_N), \quad (2)$$

where f_{Nj} is the nonlinear mixing term, which becomes zero if only one mode is excited. The coefficient Γ_{Nj} is equal to 1, except when $j = (N+1)/2$, in which case it is equal to $\frac{4}{3}$. These exceptional cases (which only occur for odd N) correspond to quasi-uncoupled supermodes, in which the wires alternate between having zero and non-zero amplitude or (in the degenerate case where $N = 1$) to an isolated wire. These modes provide no modification to the GVD, and so will not be considered further.

A set of eigenvectors \vec{x}_j for the $N = 6$ array is plotted in Fig. 2(c). Under the assumption that $\tilde{E}_j \sim e^{-i\omega t}$, the supermode dispersion operators $\hat{D}_j(i\partial_t)$ can be reconstructed ($\omega \rightarrow i\partial_t$) from

$$D_j(\omega) = D(\omega) + \chi_j C(\omega), \quad \chi_j \equiv 2 \cos\left(\frac{\pi j}{N+1}\right). \quad (3)$$

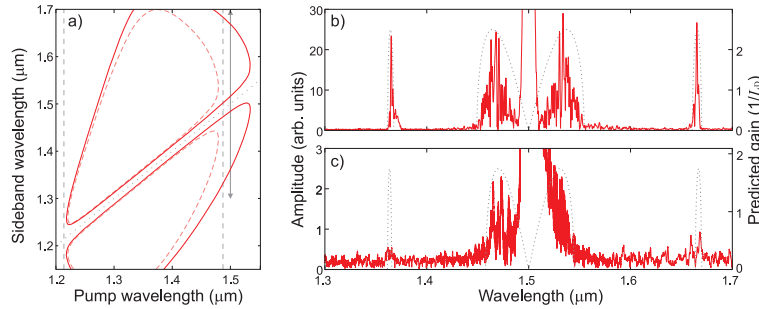


Fig. 3. (a) Predicted wavelengths of MI sidebands versus pump wavelength. Anomalous GVD of a single wire is in the region between the vertical dashed-grey lines. The dashed loops correspond to uncoupled wires, showing that no MI occurs at the $1.5\mu\text{m}$ pump. The solid loops correspond to antisymmetric supermode, showing that MI does occur. (b) Spectral output after a distance of 1.93mm , of a rectangular pulse with power $10P_0$ and duration 10ps . The overlaid prediction for gain (dotted grey line) is for $5P_0$, to allow for the effect of damping. (c) As for (b), but with free-carrier effects included. The predicted gain overlay is for $3.5P_0$.

If the dispersion of the coupling is negligible (i.e. $\partial_\omega C \approx 0$), then the supermodes have different phase velocities, but the same group velocity. If $\partial_\omega C$ is significantly different from zero (but $|\partial_\omega^2 C| \ll |\partial_\omega^2 D|$), then the group velocities of the supermodes ($\partial_\omega D_j$) are significantly different. This case has been studied experimentally and theoretically using fiber couplers (e.g. [19]). In the silicon arrays considered here $\partial_\omega^2 C$ and $\partial_\omega^2 D$ are comparable, see Figs. 2(a),(b). Therefore the GVDs ($\partial_\omega^2 D_j$) of the different supermodes are very different one from another.

The wavelength dependence of the supermode GVDs in a directional coupler ($N = 2$) and in an array ($N = 6$) are shown in Fig. 2(b) with dashed and dotted lines, respectively. If a single wire has a large normal GVD at $1.5\mu\text{m}$, then the mode corresponding to the anti-phase excitation of the two wires in the directional coupler has a strong anomalous GVD. In the $N = 6$ case, three supermodes have their GVD values pushed up into the large anomalous range, whilst the other three are pushed further into the normal. The solid color in Fig. 2(b) fills the region between the in-phase and out-of-phase modes of the $N = \infty$ array. It can be seen from Eq. 3, that the anti-phase mode always gains the largest shift towards anomalous values of GVD, whilst the in-phase mode gains the largest shift towards normal values of GVD.

The changes in the GVDs of the supermodes are reflected in the nonlinear properties of the array system. First we consider modulational instability (MI), the process which is relevant if one uses continuous-wave or relatively long pump-pulse duration. We focus on the MI of the anti-phase mode \tilde{E}_2 of the $N = 2$ array. The growth rate κ_2 (MI gain) of the perturbations confined within the \tilde{E}_2 field and having the frequency detuning ω from the pump at Ω_0 is calculated from $2\kappa_2 = \text{Im}[G_2(G_2 + 4|A|^2)]^{1/2}$, where $G_2 \equiv D_2(\omega) + D_2(-\omega)$ and $|A|$ is the initial amplitude of the anti-phase mode. Figure 3(a) shows the positions of the maxima of the MI gain vs the pump frequency. One can see that using an antisymmetric mode of a coupler significantly extends the range of the MI gain on the long wavelength side, relative to the MI in a single wire (see the dashed lines). κ_2 as a function of ω is shown in Figs. 3(b) and 3(c). One can see a broad MI band in the proximity of the pump, which is due to the GVD being anomalous, and the narrow MI bands far detuned from the pump existing due to 4th order dispersion [20, 21]. Numerical modelling of Eq. (1) fully confirms predictions of our analytical results, and shows that the free carrier effects hamper, but do not preclude observation of all MI bands. Note that techniques which sweep free carriers away from the waveguide are known,

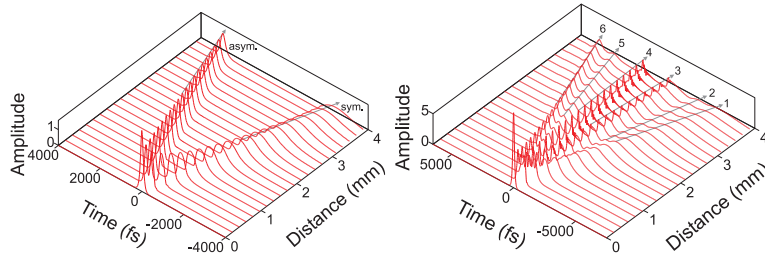


Fig. 4. a) Evolution of a pulse with peak power $15P_0$ fired into the 1st wire of a 2 wire system. The pulses in the symmetric and antisymmetric modes separate to group-velocity mismatch, with the latter becoming a soliton. b) Evolution of a pulse with peak power $150P_0$ fired into the 3rd wire of a 6 wire system. Six supermodal pulses are formed (with index j corresponding to that in Eq. 2 and figure 2(c)) The amplitude plotted is derived as $\sqrt{\sum_n |E_n|^2}$.

allowing a clearer MI picture to be seen.

If an array is pumped with femtosecond pulses, then soliton effects become important. To check for soliton propagation we integrated Eqs. (1) numerically (including linear loss, TPA and all dispersion orders). The result of sending a 100fs pulse into a single wire of the $N = 2$ array is shown in Fig. 4(a). The initial pulse splits into a pair of pulses propagating with different velocities (matching the group velocities of the two supermodes). The pulse corresponding to the in-phase supermode disperses much more rapidly than the one corresponding to the anti-phase supermode. This is because the latter experiences anomalous GVD, which is compensated for by the nonlinearity. The net result is the formation of the quasi-solitonic pulse losing its energy due to linear and nonlinear losses. Similar simulation for the $N = 6$ case, (see Fig. 4(b)), shows that the modes 4, 5 and 6 having anomalous GVD spread at a reduced pace relative to the normally dispersive modes 1, 2 and 3. This again confirms quasi-solitonic propagation regimes of the modes with anomalous GVD.

Neglecting all the terms involving ∂_t^m with $m > 2$ and assuming that the time domain overlap of the pulses corresponding to the different supermodes is negligible we find analytical expressions for the supermodal solitons:

$$\tilde{E}_j = e^{iqz} \sqrt{\frac{2(q - \chi_j c_0)}{\Gamma_{Nj}}} \operatorname{sech} \left(\sqrt{\frac{q - \chi_j c_0}{-(d_2 + \chi_j c_2)}} (t - z\chi_j c_1) \right). \quad (4)$$

The necessary condition for the soliton existence is no longer $d_2 < 0$, but $d_2 + \chi_j c_2 < 0$, thus allowing for solitons when a single wire has normal GVD ($d_2 > 0$). It is known that supermodal solitons in a two-wire system can exhibit bifurcation phenomena at high values of q , due to the influence of asymmetric nonlinear modes [22]. Spectral analysis of linear perturbations around the antisymmetric soliton solution carried out in the $N = 2$ array has not revealed instabilities in the broad domain of wavelengths and powers.

In summary, using the example of nano-sized silicon photonic wires we have shown that the GVD in waveguide arrays can vary dramatically between the supermodes, and this can be used to achieve a large anomalous GVD in a system of normally dispersive waveguides. Thus soliton propagation and frequency conversion by means of modulational instability become possible and can be initiated or suppressed by selective excitation of the desired supermodes.